Thermal Hall effect in the Kitaev-Heisenberg system with spin-phonon coupling

Shaozhi Li and Satoshi Okamoto

Phys. Rev. B **106**, 024413 — Published 14 July 2022

DOI: 10.1103/PhysRevB.106.024413

Thermal Hall Effect in the Kitaev-Heisenberg System with Spin-Phonon Coupling

Shaozhi Li* and Satoshi Okamoto
Materials Science and Technology Division, Oak Ridge National Laboratory, Oak Ridge, TN 37831, USA
(Dated: June 30, 2022)

Motivated by the giant phonon anomalies in α-$RuCl_3$ reported by Li *et al.* [Nat. Commun. **12**, 3513 (2021)], we investigate the thermal Hall effect in a Kitaev-Heisenberg system in the presence of the coupling between spins and phonons arising from chlorine atoms' vibration. We observe that the coupling modifies the relative stability between different magnetic states under a magnetic field, especially stabilizing a canted zigzag antiferromagnetic state. Remarkably, the spin-phonon interaction has distinct effects on the thermal Hall conductivity in different magnetically ordered states. For a canted zigzag state, which is relevant to α-$RuCl_3$, the spin-phonon interaction enhances the magnon excitation gap induced by a magnetic field and suppresses the thermal Hall conductivity at low temperatures. For the Kitaev spin liquid state, we find that the spin-phonon interaction reduces the excitation gap of Majorana fermions and destabilizes the quantized thermal Hall effect. Our results demonstrate a crucial role of phonon degrees of freedom to the thermal Hall effect in Kitaev materials.

I. INTRODUCTION

Phonons play a fundamental role in controlling the electronic and magnetic properties of materials [1–12]. For example, the electron-phonon interaction induces the charge-density-wave and superconductivity in the high-temperature superconductor $Ba_{0.51}K_{0.49}BiO_3$ [13]. Furthermore, phonons can couple to spins and induce the spin-Peierls transition in quasi-one-dimensional materials, such as $CuGeO_3$ [14] and TiOCl [15].

Here, we focus on α-$RuCl_3$ [16–24], a candidate material to realize the Kitaev spin liquid state [25]. A significant interplay between phonons and spins has been reported in α-$RuCl_3$ [26–29]. In α-$RuCl_3$, the edge-sharing Ru-Cl octahedra form a honeycomb lattice with an effective spin-1/2. The interaction between two nearest-neighbor pseudospins strongly depends on the Ru-Ru distance and the Ru-Cl-Ru bond angle [30]. Many experimental studies have reported the signature of spin-phonon couplings in this compound. For example, the spin-phonon coupling renormalizes phonon propagators and generates the salient Fano lineshape in the Raman spectroscopy [18, 31–34]. The coupling between phonons and Majorana fermions has been suggested to play a pivotal role in realizing the quantized thermal Hall effect [35–40].

To gain insight into the novel magnetic behavior in α-$RuCl_3$, various microscopic spin models were developed by using the density-functional theory (DFT) or fitting to inelastic neutron scattering spectra [16, 19, 41–49]. These model studies have provided significant insights, including the heat capacity and the Raman spectra. However, some important experimental features remain unexplained, such as the Fano effect in the Raman spectra [33, 34] and the sample dependence of the quantized thermal Hall effect in α-$RuCl_3$ [50]. To resolve these difficulties, the spin-phonon coupling was suggested to play an essential role. In this case, it is necessary to develop a model that includes both spin and phonon degrees of freedoms. However, compared to the Kitaev-Heisenberg model, far fewer studies exist for such a model. Recently, several studies have considered phonons in the Majoranan fermion representation to explain the Fano effect [33, 34, 39]. Such studies only considered the Kitaev-type interaction and neglected other terms that are relevant to α-$RuCl_3$. Furthermore, the effect of the spin-phonon coupling on the thermal Hall conductivity has not been clarified, while some interesting predictions have been made by analyzing a phenomenological model [51].

In this work, we develop a microscopic model with spin-phonon interactions to study the thermal Hall conductivity in α-$RuCl_3$. We consider optical phonons, which originate from the vibration of the Cl-Cl bond (shown in Fig. 1(a)). These optical phonons modify the Ru-Cl-Ru bond angle, hereby the spin-spin interaction between Ru atoms [30, 52]. A DFT study has shown that the relaxation of chlorine atoms enhances the hopping between d_{xz} and d_{yz} orbitals and suppresses the hopping between d_{xy} orbitals. As a consequence, the Heisenberg interaction is reduced by about half [30]. With these considerations in mind, we focus on the vibration of ruthenium atoms, which has been oversighted in recent phonon-related work [33, 34, 37, 38].

Our work systematically reveals the magnetic prop-

erties of both magnetically ordered states and the spin liquid state in the presence of the spin-phonon coupling in Kitaev materials. We first use the mean-field theory to study the spin-phonon interaction in the Kitaev-Heisenberg model under a magnetic field. We observe that optical phonons stabilize the canted zigzag state and destabilize the antiferromagnetic star state. Next, we use the generalized spin-wave theory to study the thermal Hall conductivity. We find that the spin-phonon interaction has distinct effects on the thermal Hall conductivity in different magnetic states. For example, in a canted zigzag state, which is relevant to α-$RuCl_3$, the spin-phonon interaction increases the magnon excitation gap and suppresses the thermal Hall conductivity at low temperatures. In other magnetic states, such as an antiferromagnetic star state, the spin-phonon interaction generates a nonmonotonic behavior in the thermal Hall conductivity. We also examined the pure Kitaev model coupled with phonons. We found that the quantized thermal Hall effect in the spin liquid state is destabilized by the spin-phonon interaction. Our results provide a guidance to understand the anomalous thermal Hall behavior of α-$RuCl_3$.

The rest of the paper is organized as follows: In Sec. II, we will describe the Kitaev-Heisenberg model with spin-phonon interaction. Detailed results will be presented in Sec. III. In Sec. III.A, we will discuss the phase diagram in the presence of the spin-phonon interaction. In Secs. III.B and III.C, we will analyze the effect of the spin-phonon interaction on the magnetic properties, including the magnetization and the thermal Hall conductivity. In addition, we will compare our simulated results with experimental data in Sec. III.D. To gain insight into the spin liquid state, we will study the Kitaev model with spin-phonon interaction in Sec. III.E. Sec. IV is devoted to further discussion and summary.

II. MODEL HAMILTONIAN

To begin with, we set up our theoretical model. Our optical phonons come from the motion of chlorine atoms in α-$RuCl_3$ as shown in Fig. 1(a). This optical phonon changes the distance d between two chlorine atoms and modifies the spin-spin interaction $J(d)$ between Ru atoms. Assuming that the variation of d is small, the interaction can be approximated as $J(d) = J(d_0)\left[1 - g(d - d_0)\right]$, where d_0 is the distance at the equilibrium position, and the spin-phonon coupling $g = -\frac{1}{J(d_0)}\frac{\partial J(d)}{\partial d}$. Including such phonon contributions, the Kitaev-Heisenberg model [53] for α-$RuCl_3$ may be modeled as $H = H_{\rm spin} + H_{\rm ph} + H_{\rm spin-ph}$, where

$$H_{\rm spin} = \sum_{\langle ij\rangle_\gamma}\left[2K\hat{S}_i^\gamma\hat{S}_j^\gamma + J\hat{\mathbf{S}}_i\cdot\hat{\mathbf{S}}_j\right] - \sum_{i,\eta} g_L\mu_B H_\eta \hat{S}_i^\eta,$$

$$H_{\rm ph} = \sum_{\langle ij\rangle}\left[\frac{M\hat{u}_{ij}^2}{2} + \frac{K_{\rm lat}\hat{u}_{ij}^2}{2}\right],$$

$$H_{\rm spin-ph} = -\sum_{\langle ij\rangle_\gamma}\hat{u}_{ij}\left[2g_K K\hat{S}_i^\gamma\hat{S}_j^\gamma + g_J J\hat{\mathbf{S}}_i\cdot\hat{\mathbf{S}}_j\right].$$

Here, $H_{\rm spin}$ describes the spin-spin interaction in the absence of the spin-phonon interaction. J and K are the nearest-neighbor Heisenberg and Kitaev couplings, respectively. These two variables are parameterized by $J = A\cos\xi$ and $K = A\sin\xi$ [54–58]. $\langle ij\rangle_\gamma$ denotes the nearest-neighbor γ bond, with $\gamma = x, y, z$. We follow Ref. [58] and set that the [111] direction in the spin space is parallel to the c axis and S^z direction is on the ac plane. H_η is the magnetic field along the η direction, which is shown in Fig. 1(b). The magnetic field strength is labeled as $|\mathbf{H}| = \sqrt{H_a^2 + H_b^2 + H_c^2}$. $H_{\rm ph}$ is the Hamiltonian for phonons. $\hat{u}_{ij}$ denotes the variation of the distance between two chlorine atoms, and $\langle\hat{u}_{ij}\rangle = d_{ij} - d_0$. M and $K_{\rm lat}$ are the mass of the chlorine atom and the elastic constant between chlorine atoms, respectively. $H_{\rm spin-ph}$ describes the spin-phonon interaction. g_K and g_J are the spin-phonon couplings for the Kitaev and Heisenberg interactions, respectively.

The ground state is obtained using the mean-field approach [58, 59] (see, also, references [60–64] therein). Specifically, we set $\hat{S}^\gamma = \langle S^\gamma\rangle + \delta\hat{S}^\gamma$ and $\hat{u} = \langle u\rangle + \delta\hat{u}$. The Hamiltonian is then rewritten as $H = \text{const} + \tilde{H}_{ph} + \tilde{H}^{(1)} + \tilde{H}^{(2)} + \tilde{H}^{(3)}$, where $\tilde{H}^{(1)}$, $\tilde{H}^{(2)}$, and $\tilde{H}^{(3)}$ include terms with one, two, and three operators, respectively. $\tilde{H}_{ph}$ is the new Hamiltonian for the harmonic phonons. $\langle S^\gamma\rangle$ and $\langle u\rangle$ are obtained by self-consistently solving $H^{(1)}$ (see supplementary material [59]). After obtaining stable spin and lattice configurations, we apply a generalized spin-wave theory to $\tilde{H}^{(2)}$ and compute the Berry curvature [59]. The thermal Hall conductivity is then calculated via $\kappa_{xy} = -\frac{k_B^2 T}{\hbar N}\sum_k^{BZ}\sum_{n=1}^{L} c_2(f_{\rm BE}(\epsilon_{nk}))\Omega_{nk}$ [65–67], where $c_2(x)$ is given by $c_2(x) = \int_0^x dt\left(\ln\frac{1+t}{t}\right)^2$, $f_{\rm BE}(\epsilon_{nk})$ is the Bose distribution function, and BZ denotes the Brillouin zone. Ω_{nk} is the Berry curvature at the momentum k for the nth band. $2L$ is the number of bands, and N is the number of the magnetic unit cell, which is labeled as a dashed-rectangular in the inset of Fig. 1. In this work, we set $N = 120\times 120$, $\hbar = k_B = 1$ and neglect three-particle interaction $\tilde{H}^{(3)}$.

III. RESULTS

A. Phase diagram

We first consider the simplest case with $g_J = g_K = g$. We assume that our optical phonons belong to the low energy phonons observed in inelastic x-ray scattering experiments [27]. The phonon frequency $\omega_{\rm ph} = \hbar\sqrt{\frac{K_{\rm lat}}{M}}$

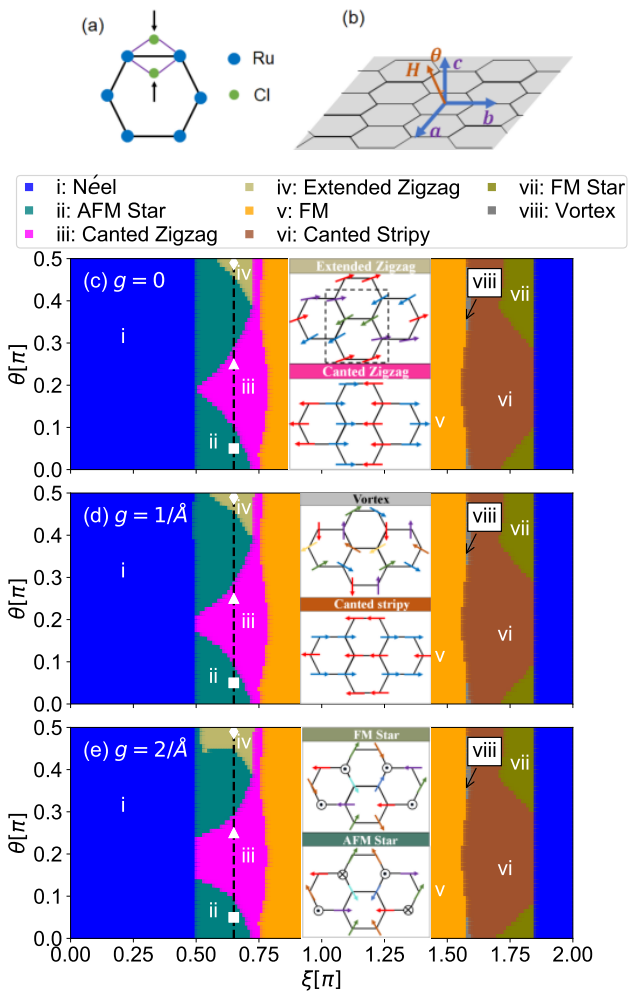

FIG. 1. (a) A sketch of chlorine atoms' vibration in α-$RuCl_3$. (b) A sketch of the Honeycomb lattice that lies on the ab plane. Panels (c)-(d) plot the phase diagrams for the spin-phonon interaction $g = 0$, $1/\text{Å}$, and $2/\text{Å}$ under a magnetic field $g_L\mu_B|\mathbf{H}| = 0.4A$, respectively. The insets in panels (c)-(e) show the spin configuration of each magnetic state when the magnetic field is along the c axis. The spin configuration is projected onto the ab plane.

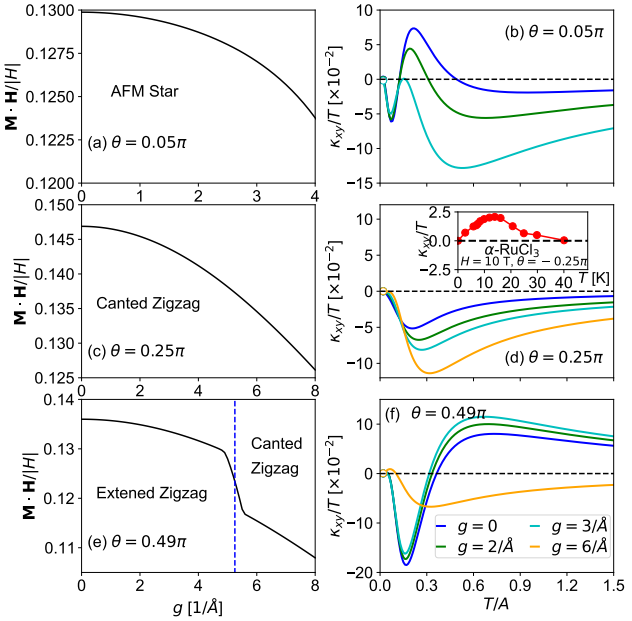

FIG. 2. The left column shows the magnetization $\mathbf{M}\cdot\mathbf{H}/|\mathbf{H}|$ along the field direction for three different values of θ. The blue dashed line in panel (c) represents the phase boundary between the extended zigzag and canted zigzag states. The right column shows the corresponding thermal Hall conductivity κ_{xy}/T as a function of temperature T. The inset in panel (e) plots the thermal Hall conductivity of α-$RuCl_3$, obtained from Ref. [68]. Here, we set $\xi = 0.65\pi$ and $g_L\mu_B|\mathbf{H}| = 0.4A$.

is estimated to be 8 meV (With $M = 35.453$ u for a Cl atom, K_{lat} is estimated to be 535.2 meV/Å^2). As reported in Ref. [27], the optical phonon energy is close to the spin-spin interaction in α-$RuCl_3$ at low temperatures, hereby we assume $A = \omega_{\text{ph}}$. Results with different values of A will be discussed later.

At zero field, the ground state of the classical spin model is a Néel antiferromagnetic (AFM) state for $-0.15\pi < \xi < 0.5\pi$, a zigzag state for $0.5\pi < \xi < 0.85\pi$, a ferromagnetic (FM) state for $0.85\pi < \xi < 1.5\pi$, and a stripy state for $1.5\pi < \xi < 1.85\pi$ [55, 59]. These ground states are changed under a magnetic field [55, 58]. In this work, we rotate the magnetic field in the ac plane (shown in Fig. 1(b)) and label the angle between the magnetic field and the c axis as θ. Figure 1(c) shows the phase diagram as a function of ξ and θ at $g_L\mu_B|\mathbf{H}| = 0.4A$ and $g = 0$. In addition to the above four magnetic states, there appear another four magnetic states, including an AFM star state (AFM Star), an extended zigzag state, a FM Star, and a vortex state (vortex) [55, 58, 59]. Remarkably, the spin-phonon interaction changes the relative stability between different magnetic states and modifies the phase diagram. As shown in Figs. 1(d) and 1(e), the spin-phonon interaction increases the regions of the canted zigzag and extended zigzag states by suppressing the AFM Star state when $0.5\pi < \xi < 0.75\pi$. By further increasing the spin-phonon interaction, the extended zigzag state is replaced by the canted zigzag state (see Fig. 2). Thus, the optical phonons stabilize the zigzag state under a magnetic field.

B. Magnetic properties

We now analyze the effect of the spin-phonon interaction on the magnetization $\mathbf{M}$ and the thermal Hall conductivity κ_{xy} in a parameter regime where the zigzag state is stable at zero field. If not stated otherwise, we set $\xi = 0.65\pi$ and $g_L\mu_B|\mathbf{H}| = 0.4A$ here. $\xi = 0.65\pi$ is indicated by dashed lines in Figs. 1(c) - 1(e). Figures 2(a) - 2(c) plot the magnetization for $\theta = 0.05\pi$, 0.25π, and

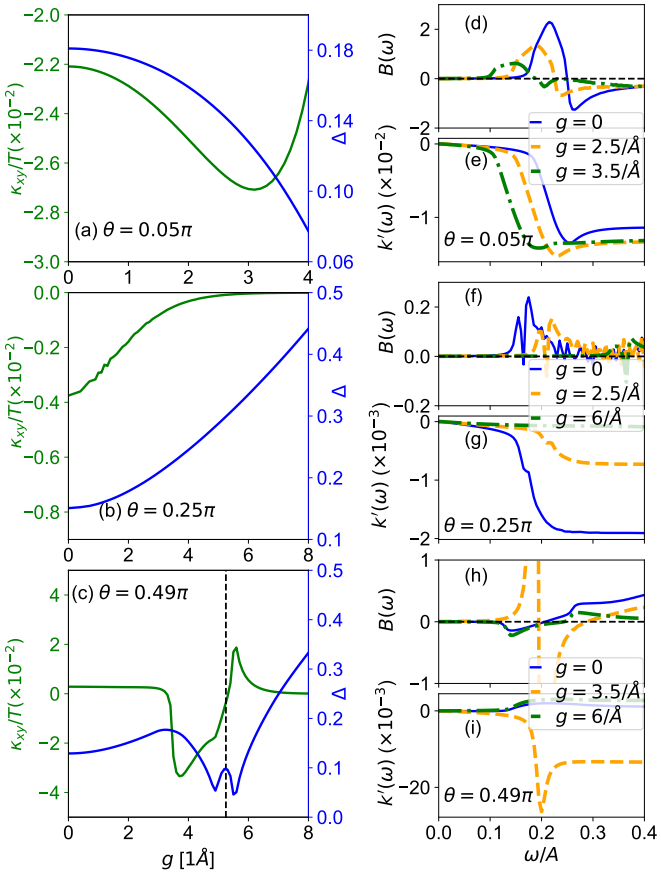

FIG. 3. The left column plots the thermal Hall conductivity κ_{xy}/T (green curve) and the energy gap Δ (blue curve) as a function of the spin-phonon interaction g for three different values of θ. The black dashed line in panel (c) represents the phase boundary between the extended zigzag state and the canted zigzag state. Panels (d), (f), and (h) plot the Berry curvature density $B(\omega)$, and panels (e), (g), and (i) plot the integrated Berry curvature density $K'(\omega)$. Here, we set $\xi = 0.65\pi$, $T = 0.04A$, and $g_L\mu_B|\mathbf{H}| = 0.4A$.

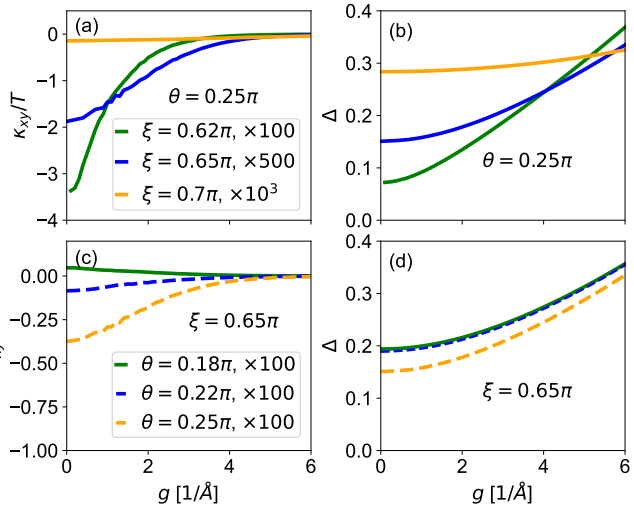

FIG. 4. Panels (a) and (c) plot the thermal Hall conductivity κ_{xy}/T for $\theta = 0.25\pi$ and $\xi = 0.65\pi$, respectively. Panels (b) and (d) plot the corresponding energy gap Δ. Here, the ground state for the selected values of θ and ξ is the canted zigzag state. The other parameters are set as $T = 0.04A$ and $g_L\mu_B|\mathbf{H}| = 0.4A$.

0.49π, respectively. The ground states for these three values of θ are the AFM Star, canted zigzag, and extended zigzag states, labeled as a white square, triangle, and diamond in Figs. 1(c) - 1(e), respectively. As shown in Figs. 2(a) - 2(c), the spin-phonon interaction suppresses the magnetization for all these three states. In addition, a first-order phase transition from the extended zigzag state to the canted zigzag state occurs at $\theta = 0.49\pi$ and $g = 5.6/\mathring{A}$, accompanied by a sudden drop in $\mathbf{M}\cdot\mathbf{H}/|\mathbf{H}|$.

Figures 2(d) - 2(f) plot the thermal Hall conductivity κ_{xy}/T as a function of temperature T for several different values of g. Interestingly, κ_{xy}/T has a distinct temperature dependence in different magnetic states. In the AFM Star (extended zigzag) state, κ_{xy}/T has three (two) extrema, while in the canted zigzag state κ_{xy}/T could have either one or two extrema, depending on the value of ξ. We note that the temperature-dependent κ_{xy}/T in the canted zigzag state is qualitatively consistent with that measured in α-$RuCl_3$ [68] (see the inset of Fig. 2(e)). It is interesting to note that κ_{xy}/T in the intermediate temperature regime ($1.2\text{A} > T > 0.3$ A) has a strong dependence on the spin-phonon interaction for all these three states.

To better visualize the change in κ_{xy}/T at low temperatures, we plot κ_{xy}/T in Figs. 3(a) - 3(c) for $T = 0.04A$. The energy gap Δ (blue curve) is also plotted in these three panels. At $\theta = 0.05\pi$ (AFM Star), $|\kappa_{xy}|/T$ is enhanced by the spin-phonon coupling when $g < 3/\text{Å}$ and suppressed when $g > 3/\text{Å}$. This nonmonotonic behavior arises from the competition between the changes in Δ and $\Omega_{n,k}$. The latter contribution can be visualized more clearly by the Berry curvature density, which is defined as $B(\omega) = \sum_{n,k}\Omega_{n,k}\delta(\omega - \epsilon_{n,k})$ and plotted in Figs. 3(d), 3(f), and 3(h). The δ function is approximated by the Lorentzian function with a width of 0.005. In the AFM Star state, the spin-phonon interaction monotonically decreases Δ, leading to an enhancement of $|\kappa_{xy}|/T$. However, the Berry curvature density near $\omega = 0.2A$ is suppressed by the spin-phonon interaction, resulting in the decrease in $|\kappa_{xy}|/T$. Figure 3(e) plots the integrated Berry curvature density $K'(\omega) = -\int_0^\omega c_2(f_{\text{BE}}(\omega'))B(\omega')d\omega'$, equivalent to the thermal Hall conductivity. It is easy to observe this competition from $K'(\omega)$ in Fig. 3(e). At $\theta = 0.25\pi$ (canted zigzag), $|\kappa_{xy}|/T$ is suppressed by the spin-phonon interaction because Δ increases and $B(\omega \approx 0.2A)$ decreases with g.

At $\theta = 0.49\pi$, κ_{xy}/T is positive and slightly suppressed by g when $g < 3/\text{Å}$. This behavior is attributed to the enhanced energy gap. Near $g = 3.2/\text{Å}$, κ_{xy}/T suddenly be-

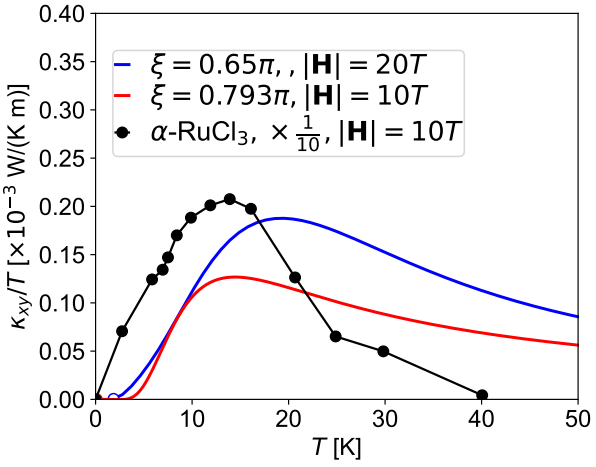

FIG. 5. The thermal Hall conductivity κ_{xy}/T as a function of temperature T. Here, we study two different models: (i) $A = 8$ meV and $\xi = 0.65\pi$; (ii) $A = 5.78$ meV and $\xi = 0.793\pi$ [69]. The thermal Hall conductivity of α-RuCl$_3$ is obtained from Ref. [68], which is renormalized by 0.1.

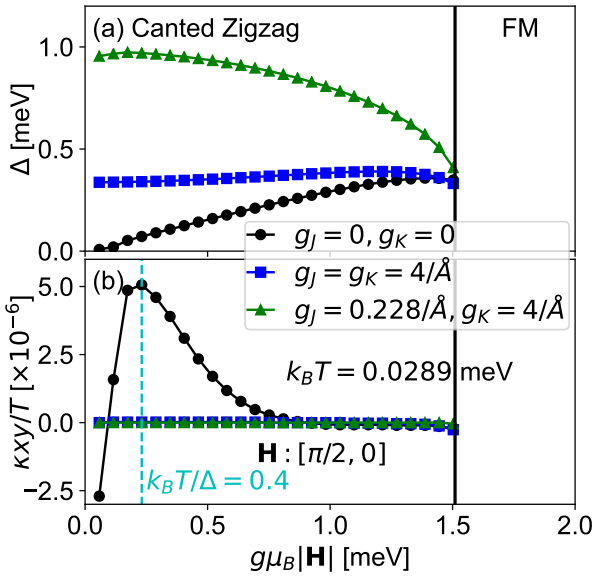

FIG. 6. (a) The energy gap as a function of the magnetic field for different spin-phonon coupling strengths. (b) The thermal Hall conductivity for different spin-phonon coupling strengths. The parameters are set as $A = 5.78$ meV and $\xi = 0.793\pi$.

comes negative and increases with g. This sudden change is due to the band crossing at the Γ point (see details in the supplementary material [59]). By further increasing g, Δ increases. At $g = 5.6/\text{Å}$, the phase transition occurs, and the ground state becomes the canted zigzag state. $|\kappa_{xy}|/T$ in this canted zigzag state has the same behavior as that shown in Fig. 3(b).

C. Canted zigzag state

We now focus on the canted zigzag state, which is relevant to α-RuCl$_3$. As shown in Fig. 3(b), the thermal Hall conductivity in the canted zigzag state is suppressed by the spin-phonon interaction. To further corroborate this trend, Fig. 4 plots κ_{xy}/T for different values of ξ and θ in the canted zigzag state at $T = 0.04A$ and $g_L\mu_B|\mathbf{H}| = 0.4A$. All the results show that κ_{xy}/T decreases as g increases, confirming that this trend is robust.

D. Relevance to α-RuCl$_3$

We compare our predicted thermal Hall conductivity with experimental results. Reference [69] proposed $K = 3.5$ meV and $J = -4.6$ meV in α-RuCl$_3$, leading to $A = 5.78$ meV and $\xi = 0.793\pi$. Figure 5 plots the temperature dependent thermal Hall conductivity of the model proposed in Ref. [69] and the model used in the previous sections in this work ($\xi = 0.65\pi$ with $A = 8$ meV). The sign of the thermal Hall conductivity depends on the orientation of the magnetic field, and one can change the sign by flipping the magnetic field. To compare with experiments, we use the absolute value of the thermal Hall conductivity. The experimental result is obtained from Ref. [68] and renormalized by 0.1. Our predicted thermal Hall conductivity of magnons is much smaller than that in α-RuCl$_3$. A similar conclusion has been made in the previous study [46]. The underestimation of the thermal Hall conductivity might be due to the fact that our spin-wave theory does not capture the quantum spin fluctuation even at low temperatures, which suppresses the ordered moment in magnetically ordered states. Moreover, the experimental data in Fig. 5 is outside of the magnetically ordered region, where quantum or thermal spin fluctuations are prominent.

Our results with $g_J = g_K$ imply that the spin-phonon interaction suppresses the thermal Hall conductivity in the canted zigzag state. However, in α-RuCl$_3$, the spin-phonon interactions could be different for different interactions [52]. To examine the validity of our conclusion, we use $g_J = 0.288/\text{Å}$ and $g_K = 4/\text{Å}$, predicted by a DFT study [52]. Figure 6 plots results for $A = 5.78$ meV and $\xi = 0.793\pi$ with three sets of g_J and g_K. Here, the magnetic field direction is fixed with $\theta = 0.25\pi$. We observe that the nonzero spin-phonon coupling increases the energy gap Δ in the canted zigzag state, hereby the thermal Hall conductivity is suppressed, consistent with our previous results with $g_J = g_K$. Yet, the precise value of Δ certainly depends on the value of g_J and g_K. For $g_J = g_K = 0$, the nonmonotonic behavior appears because of the subtle competition of the field-induced nonzero Berry curvature and magnon excitation gap with temperature.

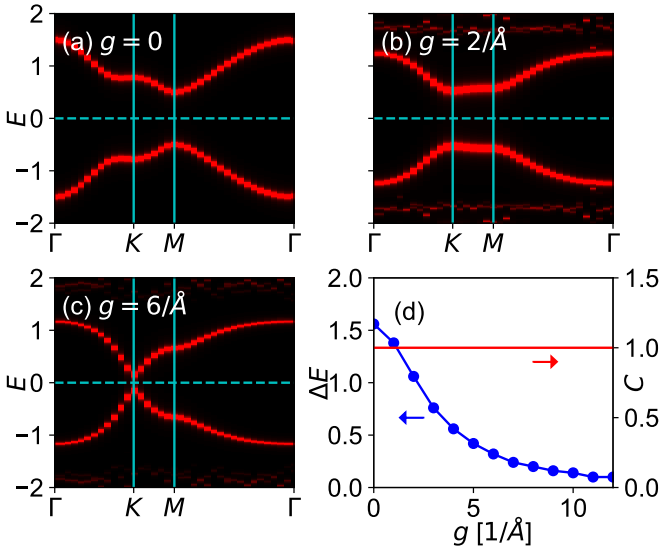

FIG. 7. Panels (a)-(c) plot the spectral functions of the Kitaev-phonon model for three different spin-phonon coupling strengths g. Panel (d) plots the energy difference ΔE (blue curve) between the energies of the lowest excited states above and below the Fermi surface at the K point. The red line represents the Chern number C.

E. Spin liquid state

Finally, we turn our attention to the spin-phonon interaction in the spin liquid state. We consider the pure Kitaev model coupled with phonons, which is described by $H = \frac{i}{2}\sum_{\langle ij\rangle} K(1-g\hat{u}_{ij})c_i c_j + \frac{i\tilde{h}}{2}\sum_{\langle\langle ij\rangle\rangle} c_i c_j + H_{\rm ph}$ [25, 70]. Here, c_i is the Majorana fermion operator at site i, and $\tilde{h}$ is an effective magnetic field. We set $K = 1$, $\tilde{h} = 0.3$, and phonon frequency $\omega_{\rm ph} = 1$ in our calculations and use the second-order perturbation theory to study this model (for details see the supplementary material [59]). Figure 7 plots the spectral functions for three different values of g. There exist energy gaps at zero energy due to an applied magnetic field. In the low-energy region, the spin-phonon interaction decreases the energy $E_{\pm}(k)$ of the lowest excited state at the K point. Here, $E_{+(-)}(k)$ represents the energy above (below) the Fermi surface at the momentum k. Figure 7(d) plots the variation of the energy difference ΔE between $E_+(K)$ and $E_-(K)$. While ΔE is decreased by the spin-phonon interaction, the Chern number C remains 1 [71, 72]. Thus, the spin-phonon interaction does not induce a topological phase transition.

The nonzero Chern number implies the quantization of the thermal Hall conductivity at low temperatures. However, when the thermal energy is close to or larger than the energy gap, the quantized thermal Hall effect is expected to disappear [73]. With increasing the spin-phonon interaction, the energy gap approaches zero, hereby the temperature range to observe the quantized thermal Hall effect is reduced to lower temperatures. Therefore, the sample-dependence of the half-integer quantized thermal Hall effect in α-$RuCl_3$ could be ascribed to the sample-dependent spin-phonon interactions [50].

IV. DISCUSSION AND SUMMARY

In this work, we studied the effect of the spin-phonon interaction on the magnetic ground state, magnon excitations, and the thermal Hall conductivity in the Kitaev-Heisenberg system. We observed that a large spin-phonon interaction stabilizes the canted zigzag state under a magnetic field. Further, the spin-phonon interaction has distinct effects on the thermal Hall conductivity in different magnetic states. In the zigzag state, the spin-phonon interaction increases the energy gap and suppresses the low temperature thermal Hall conductivity. This effect is robust with respect to model parameters as long as the canted zigzag state is stabilized. In the Kitaev spin liquid state, we find that the spin-phonon interaction destabilizes the quantized thermal Hall effect by suppressing Majorana excitation gap. Our results provide crucial guidance to understand thermal Hall conductivity in Kitaev materials, including α-$RuCl_3$ and $Na_2Co_2TeO_6$ [74].

In this work, we consider optical phonons arising from the displacement of chlorine atoms. It would be important to study acoustic phonons, which involve the displacement of ruthenium atoms, and examine how these phonons modify the magnetic properties in α-$RuCl_3$.

ACKNOWLEDGMENTS

This research was supported by the U.S. Department of Energy, Office of Science, National Quantum Information Science Research Centers, Quantum Science Center. This research used resources of the Compute and Data Environment for Science (CADES) at the Oak Ridge National Laboratory, which is supported by the Office of Science of the U.S. Department of Energy under Contract No. DE-AC05-00OR22725.

* lishaozhiphys@gmail.com

[1] W. Weber, Phys. Rev. Lett. **58**, 1371 (1987).
[2] M. Lazzeri, C. Attaccalite, L. Wirtz, and F. Mauri, Phys. Rev. B **78**, 081406(R) (2008).
[3] D. J. J. Marchand, G. De Filippis, V. Cataudella, M. Berciu, N. Nagaosa, N. V. Prokof'ev, A. S. Mishchenko, and P. C. E. Stamp, Phys. Rev. Lett. **105**, 266605 (2010).

[4] E. A. Nowadnick, S. Johnston, B. Moritz, R. T. Scalettar, and T. P. Devereaux, Phys. Rev. Lett. **109**, 246404 (2012).

[5] S. Li, E. Khatami, and S. Johnston, Phys. Rev. B **95**, 121112(R) (2017).

[6] J. Sous, M. Chakraborty, R. V. Krems, and M. Berciu, Phys. Rev. Lett. **121**, 247001 (2018).

[7] N. C. Costa, K. Seki, S. Yunoki, and S. Sorella, Communications Physics **3**, 80 (2020).

[8] N. C. Costa, K. Seki, and S. Sorella, Phys. Rev. Lett. **126**, 107205 (2021).

[9] C.-C. Lee, J.-Y. Chiu, Y. Yamada-Takamura, and T. Ozaki, Phys. Rev. B **104**, 064114 (2021).

[10] A. Sapkota, T. C. Sterling, P. M. Lozano, Y. Li, H. Cao, V. O. Garlea, D. Reznik, Q. Li, I. A. Zaliznyak, G. D. Gu, and J. M. Tranquada, Phys. Rev. B **104**, 014304 (2021).

[11] S. Li and S. Johnston, npj Quantum Materials **5**, 40 (2020).

[12] B. Xing, W.-T. Chiu, D. Poletti, R. T. Scalettar, and G. Batrouni, Phys. Rev. Lett. **126**, 017601 (2021).

[13] C. H. P. Wen, H. C. Xu, Q. Yao, R. Peng, X. H. Niu, Q. Y. Chen, Z. T. Liu, D. W. Shen, Q. Song, X. Lou, Y. F. Fang, X. S. Liu, Y. H. Song, Y. J. Jiao, T. F. Duan, H. H. Wen, P. Dudin, G. Kotliar, Z. P. Yin, and D. L. Feng, Phys. Rev. Lett. **121**, 117002 (2018).

[14] M. Hase, I. Terasaki, and K. Uchinokura, Phys. Rev. Lett. **70**, 3651 (1993).

[15] M. Shaz, S. van Smaalen, L. Palatinus, M. Hoinkis, M. Klemm, S. Horn, and R. Claessen, Phys. Rev. B **71**, 100405(R) (2005).

[16] K. W. Plumb, J. P. Clancy, L. J. Sandilands, V. V. Shankar, Y. F. Hu, K. S. Burch, H.-Y. Kee, and Y.-J. Kim, Phys. Rev. B **90**, 041112(R) (2014).

[17] Y. Kubota, H. Tanaka, T. Ono, Y. Narumi, and K. Kindo, Phys. Rev. B **91**, 094422 (2015).

[18] L. J. Sandilands, Y. Tian, K. W. Plumb, Y.-J. Kim, and K. S. Burch, Phys. Rev. Lett. **114**, 147201 (2015).

[19] R. D. Johnson, S. C. Williams, A. A. Haghighirad, J. Singleton, V. Zapf, P. Manuel, I. I. Mazin, Y. Li, H. O. Jeschke, R. Valentí, and R. Coldea, Phys. Rev. B **92**, 235119 (2015).

[20] J. A. Sears, M. Songvilay, K. W. Plumb, J. P. Clancy, Y. Qiu, Y. Zhao, D. Parshall, and Y.-J. Kim, Phys. Rev. B **91**, 144420 (2015).

[21] H. B. Cao, A. Banerjee, J.-Q. Yan, C. A. Bridges, M. D. Lumsden, D. G. Mandrus, D. A. Tennant, B. C. Chakoumakos, and S. E. Nagler, Phys. Rev. B **93**, 134423 (2016).

[22] A. Koitzsch, C. Habenicht, E. Müller, M. Knupfer, B. Büchner, H. C. Kandpal, J. van den Brink, D. Nowak, A. Isaeva, and T. Doert, Phys. Rev. Lett. **117**, 126403 (2016).

[23] M. G. Yamada, H. Fujita, and M. Oshikawa, Phys. Rev. Lett. **119**, 057202 (2017).

[24] Y. Kasahara, T. Ohnishi, Y. Mizukami, O. Tanaka, S. Ma, K. Sugii, N. Kurita, H. Tanaka, J. Nasu, Y. Motome, T. Shibauchi, and Y. Matsuda, Nature **559**, 227 (2018).

[25] A. Kitaev, Annals of Physics **321**, 2 (2006), january Special Issue.

[26] R. Hentrich, A. U. B. Wolter, X. Zotos, W. Brenig, D. Nowak, A. Isaeva, T. Doert, A. Banerjee, P. Lampen-Kelley, D. G. Mandrus, S. E. Nagler, J. Sears, Y.-J. Kim, B. Büchner, and C. Hess, Phys. Rev. Lett. **120**, 117204 (2018).

[27] H. Li, T. T. Zhang, A. Said, G. Fbbris, D. G. Mazzone, Q. J. Yan, D. B. Mandrus, G. Halász, S. Okamoto, M. P. M. Dean, H. N. Lee, and H. Miao, Nature Communications **12**, 3513 (2021).

[28] S. Mu, K. D. Dixit, X. Wang, D. L. Abernathy, H. Cao, S. E. Nagler, J. Yan, P. Lampen-Kelley, D. Mandrus, C. A. Polanco, L. Liang, G. B. Halász, Y. Cheng, A. Banerjee, and T. Berlijn, Phys. Rev. Research **4**, 013067 (2022).

[29] B. W. Lebert, S. Kim, D. A. Prishchenko, A. A. Tsirlin, A. H. Said, A. Alatas, and Y.-J. Kim, "Acoustic phonon dispersion of $\alpha-RuCl_3$," ArXiv: 2201.09959 (2022).

[30] H.-S. Kim and H.-Y. Kee, Phys. Rev. B **93**, 155143 (2016).

[31] G. Li, X. Chen, Y. Gan, F. Li, M. Yan, F. Ye, S. Pei, Y. Zhang, L. Wang, H. Su, J. Dai, Y. Chen, Y. Shi, X. Wang, L. Zhang, S. Wang, D. Yu, F. Ye, J.-W. Mei, and M. Huang, Phys. Rev. Materials **3**, 023601 (2019).

[32] A. Glamazda, P. Lemmens, S.-H. Do, Y. S. Kwon, and K.-Y. Choi, Phys. Rev. B **95**, 174429 (2017).

[33] K. Feng, S. Swarup, and N. B. Perkins, "Footprints of the kitaev spin liquid in the fano lineshapes of the raman active optical phonons," ArXiv: 2108.08878 (2021).

[34] A. Metavitsiadis, W. Natori, J. Knolle, and W. Brenig, "Optical phonons coupled to kitaev spin liquid," ArXiv: 2103.0982 (2021).

[35] M. Ye, G. B. Halász, L. Savary, and L. Balents, Phys. Rev. Lett. **121**, 147201 (2018).

[36] Y. Vinkler-Aviv and A. Rosch, Phys. Rev. X **8**, 031032 (2018).

[37] A. Metavitsiadis and W. Brenig, Phys. Rev. B **101**, 035103 (2020).

[38] M. Ye, R. M. Fernandes, and N. B. Perkins, Phys. Rev. Research **2**, 033180 (2020).

[39] K. Feng, M. Ye, and N. B. Perkins, Phys. Rev. B **103**, 214416 (2021).

[40] A. Ruiz, N. P. Breznay, M. Li, I. Rousochatzakis, A. Allen, I. Zinda, V. Nagarajan, G. Lopez, Z. Islam, M. H. Upton, J. Kim, A. H. Said, X.-R. Huang, T. Gog, D. Casa, R. J. Birgeneau, J. D. Koralek, J. G. Analytis, N. B. Perkins, and A. Frano, Phys. Rev. B **103**, 184404 (2021).

[41] H.-S. Kim, V. S. V., A. Catuneanu, and H.-Y. Kee, Phys. Rev. B **91**, 241110(R) (2015).

[42] S. M. Winter, Y. Li, H. O. Jeschke, and R. Valentí, Phys. Rev. B **93**, 214431 (2016).

[43] L. J. Sandilands, C. H. Sohn, H. J. Park, S. Y. Kim, K. W. Kim, J. A. Sears, Y.-J. Kim, and T. W. Noh, Phys. Rev. B **94**, 195156 (2016).

[44] Y. S. Hou, H. J. Xiang, and X. G. Gong, Phys. Rev. B **96**, 054410 (2017).

[45] W. Wang, Z.-Y. Dong, S.-L. Yu, and J.-X. Li, Phys. Rev. B **96**, 115103 (2017).

[46] J. Cookmeyer and J. E. Moore, Phys. Rev. B **98**, 060412 (2018).

[47] T. Suzuki and S.-i. Suga, Phys. Rev. B **97**, 134424 (2018).

[48] C. Eichstaedt, Y. Zhang, P. Laurell, S. Okamoto, A. G. Eguiluz, and T. Berlijn, Phys. Rev. B **100**, 075110 (2019).

[49] P. Laurell and S. Okamoto, npj quantum materials **5**, 2 (2020).

[50] M. Yamashita, J. Gouchi, Y. Uwatoko, N. Kurita, and H. Tanaka, Phys. Rev. B **102**, 220404(R) (2020).

[51] M. Ye, G. B. Halász, L. Savary, and L. Balents, Phys. Rev. Lett. **121**, 147201 (2018).

[52] D. A. S. Kaib, S. Biswas, K. Riedl, S. M. Winter, and R. Valentí, Phys. Rev. B **103**, L140402 (2021).

[53] L. E. Chern, F. L. Buessen, and Y. B. Kim, **6**, 33 (2021).

[54] J. c. v. Chaloupka, G. Jackeli, and G. Khaliullin, Phys. Rev. Lett. **105**, 027204 (2010).

[55] L. Janssen, E. C. Andrade, and M. Vojta, Phys. Rev. Lett. **117**, 277202 (2016).

[56] G.-W. Chern, Y. Sizyuk, C. Price, and N. B. Perkins, Phys. Rev. B **95**, 144427 (2017).

[57] P. M. Cônsoli, L. Janssen, M. Vojta, and E. C. Andrade, Phys. Rev. B **102**, 155134 (2020).

[58] S. Koyama and J. Nasu, Phys. Rev. B **104**, 075121 (2021).

[59] See Supplemental Material at http://****** for the detailed methodology and the results of the extended Kitaev-Heisenberg model..

[60] S. M. Winter, K. Riedl, P. A. Maksimov, A. L. Chernyshev, A. Honecker, and R. Valentí, Nature Communications **8**, 1152 (2017).

[61] K. Ran, J. Wang, W. Wang, Z.-Y. Dong, X. Ren, S. Bao, S. Li, Z. Ma, Y. Gan, Y. Zhang, J. T. Park, G. Deng, S. Danilkin, S.-L. Yu, J.-X. Li, and J. Wen, Phys. Rev. Lett. **118**, 107203 (2017).

[62] L. Janssen, E. C. Andrade, and M. Vojta, Phys. Rev. B **96**, 064430 (2017).

[63] A. Mook, J. Henk, and I. Mertig, Phys. Rev. B **99**, 014427 (2019).

[64] E. C. Andrade, L. Janssen, and M. Vojta, Phys. Rev. B **102**, 115160 (2020).

[65] H. Katsura, N. Nagaosa, and P. A. Lee, Phys. Rev. Lett. **104**, 066403 (2010).

[66] R. Matsumoto, R. Shindou, and S. Murakami, Phys. Rev. B **89**, 054420 (2014).

[67] Y.-f. Yang, G.-M. Zhang, and F.-C. Zhang, Phys. Rev. Lett. **124**, 186602 (2020).

[68] T. Yokoi, S. Ma, Y. Kasahara, T. Shibauchi, N. Kurita, H. Tanaka, J. Nasu, Y. Motome, C. Hickey, S. Trebst, and Y. Matsuda, Science **373**, 568 (2021).

[69] A. Banerjee, C. A. Bridges, J.-Q. Yan, A. A. Aczel, L. Li, M. B. Stone, G. E. Granroth, M. D. Lumsden, Y. Yiu, J. Knolle, S. Bhattacharjee, D. L. Kovrizhin, R. Moessner, D. A. Tennant, D. G. Mandrus, and S. E. Nagler, Nature Materials **15**, 733 (2016).

[70] M. G. Yamada, npj Quantum Materials **5**, 82 (2020).

[71] T. Fukui, Y. Hatsugai, and H. Suzuki, Journal of the Physical Society of Japan **74**, 1674 (2005).

[72] T. I. Vanhala, T. Siro, L. Liang, M. Troyer, A. Harju, and P. Törmä, Phys. Rev. Lett. **116**, 225305 (2016).

[73] F. Mirmojarabian, M. Kargarian, and A. Langari, Phys. Rev. B **101**, 115116 (2020).

[74] X. Hong, M. Gillig, R. Hentrich, W. Yao, V. Kocsis, A. R. Witte, T. Schreiner, D. Baumann, N. Pérez, A. U. B. Wolter, Y. Li, B. Büchner, and C. Hess, Phys. Rev. B **104**, 144426 (2021).